Multiple Morphologies, Phase Transitions, and Cross-Linking of Crew-Cut Aggregates of Polybutadiene-*block*-poly(2-vinylpyridine) Diblock Copolymers

Andreas Walther,* Anja S. Goldmann, Ram Sai Yelamanchili,† Markus Drechsler, Holger Schmalz, Adi Eisenberg,‡ and Axel H. E. Müller*

Makromolekulare Chemie II and Bayreuther Zentrum für Kolloide and Grenzflächen, Universität Bayreuth, D-95440 Bayreuth, Germany

Received November 25, 2007; Revised Manuscript Received January 28, 2008

ABSTRACT: We describe detailed investigations on the self-assembly of polybutadiene-*block*-poly(2-vinylpyridine) diblock copolymers into so-called crew-cut micellar aggregates in aqueous media. Three analogous diblock copolymers with different short segments of poly(2-vinylpyridine) were synthesized via anionic polymerization. The self-assembled aggregates are studied in dioxane/water mixtures by means of dynamic light scattering and transmission electron microscopy. Depending on the added volume fraction of water, spherical micelles, branched cylindrical micelles, and vesicles can be found. These aggregates can be cross-linked in a facile fashion using a UV photoinitiator. The structures of the crew-cut aggregates remain intact during cross-linking, yielding stabilized polymeric nanoparticles. A transfer of these nanoparticles into common, only slightly selective solvents, in which no aggregates or different type of aggregates would exist without cross-linking, is possible. The cross-linked nanoparticle structures remain unchanged during this process. Moreover, a new pathway for the phase transition of cylindrical micelles to vesicles was found and is elucidated.

Introduction

Amphiphilic block copolymers are able to self-assemble into discrete well-defined nanoarchitectures upon exposure to selective solvents.[1–4] The properties and the aggregate structures can be modified via, e.g., changing the chemical composition of the constituting blocks.[5–9] Pioneering work by Eisenberg and others has given a deep insight in the formation mechanism,[10–13] structural variety[9,14,15] and application possibilities of self-assembled aggregates.[16–19] A major interest in this research has been devoted to anionic polyelectrolyte systems, such as the polystyrene-*block*-poly([meth]acrylic acid) (PS-*b*-P[M]AA) systems.

In the field of cationically charged block copolymers and their self-assembly, in particular Förster and Armes[20–24] have reported results on micellar aggregation and properties. For instance, Förster et al. studied the fusion of micelles of polybutadiene-*block*-poly(2-vinylpyridine) (PB-*b*-P2VP) on different substrates via scanning force microscopy.[25] Furthermore, spherical aggregates were used for the templated synthesis of nanoporous silica.[26] Spherical micelles of quaternized PS-*b*-P4VP type in aqueous solution were reported by Selb[27,28] and Eisenberg.[29,30] In addition to that, pH-induced phase transitions of PS-*b*-P4VP in DMF/H_2O mixtures were investigated.[31] In general, however, the solution studies of block copolymers containing vinylpyridine segments were mainly focused on inverse micelles in organic solvents based on polystyrene as hydrophobic block.[32–36] Concerning applications, inverse micelles were, for instance, used for templating inorganic nanoparticles inside the micellar core and subsequent catalytic reactions.[37] Very high turnover rates, high activities, and long-term stability were found for the Pd-catalyzed Heck reactions using Pd nanoparticles embedded into the P4VP core of inverse PB-*b*-P4VP micelles.[37] Vinylpyridine has extremely good coordination properties for metal ions and was used to create various catalytically active nanoparticles, such as Au[38], Pd[39], Co[40]. Recently, arrays of PS-*b*-P4VP micelles were used to create single-walled carbon nanotubes, demonstrating the versatility of the structures.[41]

One of the major drawbacks of self-assembled systems when aiming at applications, for instance in catalysis, is the fact that the structures depend on the type of solvent used. The tendency of forming defined aggregates is low when the block copolymer is exposed to a good solvent for both blocks, thus limiting the application range of nanoreactors or nanocontainers. For instance, micelles with polystyrene as inner block disassemble in most organic solvents and are thus not of wide applicability. Therefore, the cross-linking of block copolymer micelles and vesicles may serve as an alternative. Various efforts have been undertaken to cross-link the shell or the core of self-assembled nanoobjects.[42–44] In the case of polybutadiene containing block copolymers, the cross-linking is generally possible via γ-irradiation, radical reactions or "cold vulcanization" using S_2Cl_2.[45–47] Recently, Maskos[48] reported on the cross-linking of micelles based on polybutadiene-*block*-poly(ethylene oxide) block copolymers using γ-irradiation.

Here, we present a systematic investigation of the phase transitions, morphological variety and facile UV cross-linking of PB-*b*-P2VP diblock copolymer aggregates. The two blocks of this diblock copolymer combine two advantageous features, i.e., the ability to cross-link the structure and the chelating properties of P2VP. Thus, the formed structures and their cross-linked analogues may be of wide applicability.

We demonstrate that cross-linking of the PB domains in various kinds of aggregates based on PB-*b*-P2VP diblock copolymers can be easily accomplished with a UV photoinitiator. In contrast to a γ-source, photoinitiators are readily available and can thus find widespread use, resembling a major advantage. Additionally, detailed investigations of the aggregate morphologies of PB-*b*-P2VP diblock copolymers crew-cut systems in aqueous solvent mixtures will be reported. Furthermore, a new pathway for the phase transition from branched cylindrical micelles to vesicles will be described, which is of

* Corresponding authors. E-mail: Andreas.Walther@uni-bayreuth.de; Axel.Mueller@uni-bayreuth.de.
† Anorganische Chemie I, Universität Bayreuth, D-95440 Bayreuth, Germany.
‡ Department of Chemistry, McGill University, 801 Sherbrooke Street West, Montreal, Quebec H3A 2K6, Canada.

10.1021/ma7026148 CCC: $40.75
Published on Web 04/05/2008

fundamental importance for the study of diblock copolymer aggregates.

Experimental Section

Materials. Tetrahydrofuran (Merck, p.a.) was purified by successive distillation over CaH_2 and potassium and kept under dry nitrogen before usage. 2-Vinylpyridine (Acros, 97%) was distilled from CaH_2 under nitrogen. Subsequently, 2-vinylpyridine was degassed three times via freeze–pump–thaw cycles using a high vacuum line ($10^{-4}-10^{-5}$ mbar), stirred over Et_3Al for 2 h and condensed into storage ampoules. Butadiene (Linde) was passed over columns with molecular sieve and activated alumina, followed by storage over Bu_2Mg under purified nitrogen before use. Dioxane (Aldrich, p.a.), Lucirin TPO (BASF), *sec*-BuLi (Acros, 1.3 M in cyclohexane/hexane: 92/8), Bu_2Mg (Aldrich, 1 M in heptane), Et_3Al (Aldrich, 1 M in hexanes) were used as received. Lucirin TPO is courtesy of BASF SE.

Synthesis. The synthesis of the polybutadiene-*block*-poly(2-vinylpyridine) diblock copolymers was accomplished via sequential living anionic polymerization of the corresponding monomers in THF using *sec*-BuLi as initiator. Prior to the reaction the used THF was treated with *sec*-BuLi at −40 °C followed by stirring overnight at room temperature in order to produce alkoxides to stabilize the living polybutadiene. Butadiene polymerization was initiated with *sec*-BuLi at −70 °C, and butadiene was allowed to polymerize at −10 °C for 8 h. After subsequent cooling to −70 °C 2-vinylpyridine was added to the reaction mixture. After 1 h reaction time the polymerization was terminated with degassed methanol, and the product precipitated in a water/methanol mixture. In order to produce a series of diblock copolymers with identical PB block but varying P2VP block lengths, samples were taken during 2VP polymerization at different conversions.

Mass Spectrometry. MALDI-TOF MS analysis was performed on a Bruker Reflex III equipped with a 337 nm N2 laser and 20 kV acceleration voltage. The number-average molecular weight, M_n, of the sample was determined in the linear mode.

Preparation of Micellar Aggregates. The micellar solutions were usually prepared by stepwise dialysis of dioxane solutions against water/dioxane mixtures of desired compositions. Only in the case of studying the phase transition, slow addition of water instead of dialysis was used. This allows a higher accuracy in terms of concentration and solvent composition. In all cases Millipore water was used.

Cross-Linking. Cross-linking of the micellar solutions (0.025−0.5 wt %) in dioxane/water mixtures of any composition was accomplished by a UV initiator (0.2–5 mg/mL), Lucirin TPO. Prior to cross-linking with a standard UV Lamp (cutoff < 350 nm) for 2–6 h, the sample was allowed to equilibrate for 6–24 h at room temperature.

Gel Permeation Chromatography (GPC). GPC measurements were performed at room temperature on a system with PSS SDVgel columns (30 × 8 mm, 5 μm particle size) with 10^2, 10^3, 10^4, and 10^5 Å pore sizes using RI and UV detection (λ = 254 nm). THF was used as eluent (flow rate 1.0 mL/min) and the WinGPC software was used for data evaluation. Prior to measurements the samples were filtrated using 0.2 μm PTFE filters.

Dynamic Light Scattering (DLS). Dynamic light scattering was performed on an ALV DLS/SLS-SP 5022F compact goniometer system with an ALV 5000/E cross-correlator and a He–Ne laser (λ_0 = 632.8 nm). Prior to the light scattering measurements the sample solutions were filtered using Millipore or Roth filters (housing: polypropylene; membrane: polytetrafluoroethylene) with a pore size of 0.45–1 μm. All samples were analyzed at high dilution. The data evaluation of the dynamic light scattering measurements was performed applying the CONTIN algorithm,[49] which yields an intensity-weighted distribution of decay times after an inverse Laplace transformation of the intensity autocorrelation function. The polydispersities were determined from unimodal peaks via the cumulant method.

Transmission Electron Microscopy (TEM). A droplet of the cross-linked micellar solution was placed on a Formvar coated copper grid and most of the liquid was removed by blotting with a filter paper. Subsequently, bright-field TEM was performed on Zeiss CEM 902 and Zeiss EM 922 OMEGA FE-TEMs operating at 80 and 200 kV, respectively.

For *cryogenic* transmission electron microscopy (*cryo*-TEM) studies, a drop of the sample dissolved in THF was put on a lacey carbon transmission electron microscopy (TEM) grid, where most of the liquid was removed with blotting paper, leaving a thin film stretched over the lace. The specimens were instantly vitrified by rapid immersion into liquid nitrogen in a temperature controlled freezing unit (Zeiss Cryobox, Zeiss NTS GmbH, Oberkochen, Germany). The temperature was monitored and kept constant in the chamber during all of the sample preparation steps. After freezing the specimens, the specimen was inserted into a cryo-transfer holder (CT3500, Gatan, München, Germany) and transferred to a Zeiss EM 922 OMEGA FE-TEM. Examinations were carried out at temperatures around 90 K. The transmission electron microscope was operated at an acceleration voltage of 200 kV. Zero-loss filtered images (ΔE = 0 eV) were taken under reduced dose conditions (100–1000 e/nm^2). All images were registered digitally by a bottom mounted CCD camera system (Ultrascan 1000, Gatan) combined and processed with a digital imaging processing system (Gatan Digital Micrograph 3.9 for GMS 1.4).

Table 1. Polymer Characterization

sample code[a]	DP_n	$M_{n,NMR}$[b] (kg/mol)	$M_{n,GPC}$[c] (kg/mol)
B80V20	$PB_{721}-P2VP_{93}$	48.7	66.8 (1.02)
B87V13	$PB_{721}-P2VP_{56}$	44.9	66.4 (1.02)
B90V10	$PB_{721}-P2VP_{39}$	43.1	66.3 (1.02)

[a] The numbers denote the weight fractions in percent. [b] Molecular weight as calculated using the true molecular weight of the PB precursor, as determined by MALDI-ToF and the weight fractions as determined by ^{1}H NMR. [c] Molecular weights as determined by THF GPC using a polystyrene calibration curve. The polydispersity index is given in brackets.

Results and Discussion

Polymer Synthesis and Molecular Characterization. Three different polybutadiene-*block*-poly(2-vinylpyridine) (PB-*b*-P2VP) diblock copolymers were synthesized via sequential living anionic polymerization in THF using the same polybutadiene precursor with a predominant 1,2-structure (89% according to ^{1}H NMR). During the polymerization of the second block several samples were taken in order to obtain diblock copolymers with varying block lengths for the P2VP block. With this method it was possible to obtain a series of diblock copolymers, allowing a systematic study of the influence of the chain length on the aggregate structures formed. Table 1 shows a summary of the molecular characteristics of the different block copolymers.

The molecular weights were calculated based on the absolute molecular weight of the PB precursor, determined by MALDI-TOF mass spectrometry (see Figure 1a) in combination with the monomer unit weight fractions from ^{1}H NMR spectra of different diblock copolymers. All polymers were designed to have a relatively short P2VP block in order to access the crew-cut regime for the micellar aggregates and to create a large variety of different structures. The polybutadiene precursor and the block copolymers exhibit both narrow molecular weight distributions as can be judged from the GPC elution traces in THF (see Figure 1b). Upon addition of the second monomer, a distinct shift in the elution peak can be observed, corresponding to an increase in molecular weight and an extension of the polybutadiene to a diblock copolymer. Only a moderate shift of the peaks can be found within the series of the PB-*b*-P2VP diblock copolymers, which is, however, expected due to the interdependency of the increase in hydrodynamic radius and the adsorption of the poly(2-vinylpyridine) units onto the columns. The enlargement in hydrodynamic volume, caused by the increase in molecular weight, is somewhat counterbalanced

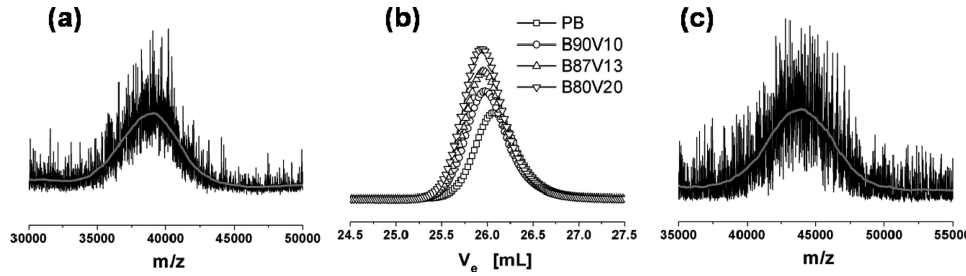

Figure 1. (a) MALDI-TOF spectrum obtained for the polybutadiene precursor after completion of the polymerization of the first block. (b) THF GPC elution traces of the polybutadiene precursor and the diblock copolymers. (c) MALDI-TOF spetrum obtained for B90V10.

by the rising adsorption. To further prove a complete blocking efficiency upon addition of the second monomer, a MALDI-TOF analysis of the diblock copolymer having the shortest P2VP chain was performed. The polybutadiene and the diblock copolymer B90V10 are structurally most analogous within the series and are thus expected to undergo ionization with a similar efficiency. The corresponding spectrum (see Figure 1c) shows a complete shift of the main peak of the polybutadiene precursor to higher molecular weights for the diblock copolymer, B90V10. Any remaining polybutadiene precursor cannot be identified and we can thus indeed conclude a full initiation of the second block. The determined number-average molecular weight, M_n, changes to 43.7 kg/mol, which is in excellent agreement with the calculated molecular weight based on the ^{1}H NMR of the diblock.

Aggregate Morphologies. Despite the low glass transition temperature of the polybutadiene, the diblock copolymers are not directly soluble in acidic water. This is presumably due to the large PB fraction in the diblock copolymers. Therefore, stepwise dialysis or slow addition of water was chosen to prepare the micellar aggregates. Due to the strong insolubility of polybutadiene in water, micellar aggregation can be induced by changing the solvent quality from a good solvent (i.e., dioxane) for both blocks to a selective solvent. Neutral water was used instead of acidic water in order to minimize charging of the P2VP chains during dialysis. It is expected that charged P2VP chains occupy more space due to electrostatic repulsion than uncharged ones, which may be unfavorable for the development of crew-cut aggregates, like wormlike micelles and vesicles. However, in the last stage of the process and if fully water-soluble structures are to be obtained, one has to dialyze against acidic water in order to allow for a sufficient stabilization of the P2VP chains, as P2VP is insoluble in water at neutral pH.

First investigations were focused on the kind of aggregates that can be found at high water concentrations. Results from Eisenberg and others had shown that the usual phase transitions start from unimers to spherical micelles to wormlike micelles and then to vesicles upon addition of water to dioxane solution of amphiphilic block copolymers. Hence, a variety of structures at low water concentration can only be expected for diblock copolymers forming vesicles at high water concentrations (here, dioxane/water = 1/1).

Figures 2, 3, and 4 show dynamic light scattering data and transmission electron micrographs of the aggregates formed by the diblock copolymers. The TEM micrographs were acquired after cross-linking a 0.25 wt % solution of the diblock copolymer in dioxane/water (1/1 v/v or 5/3 v/v) mixtures. Cross-linking of the particles is necessary to allow an imaging of the structures, as un-cross-linked particles often tend to disassemble and form films upon deposition on the TEM grids. The successful cross-linking will be shown in the following section of this publication. At this point it may just be mentioned that the aggregates remain structurally unaffected during the cross-linking process using a UV photoinitiator.

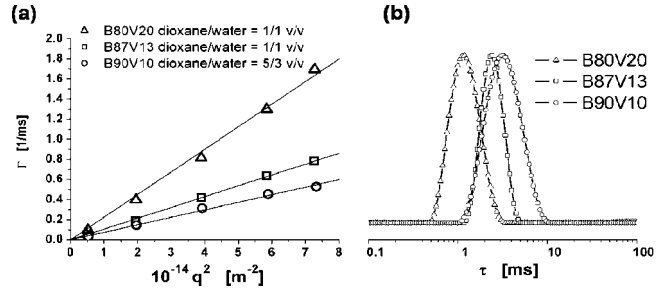

Figure 2. (a) Dependence of the decay rate on the scattering vector for the aggregates formed by the different diblock copolymers, as indicated in the graphs. The diffusion coefficients were determined from the slopes of the fitted lines. (b) Decay time distributions as obtained by CONTIN analysis at 90°. The measurements were conducted at 0.25 wt % in dioxane/water (1/1 and 5/3 v/v).

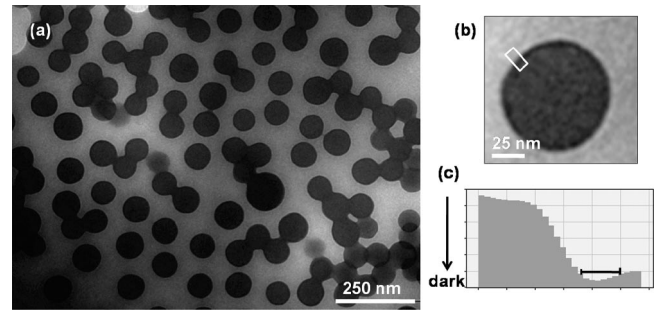

Figure 3. (a) TEM micrograph of B80V20 aggregates, which were photo-cross-linked in a dioxane/water (1:1) mixture (0.25 wt %). The sample was deposited onto a Formvar-coated copper grid. (c) Section analysis of the white area of the magnified TEM image (b). The horizontal bar in image (c) indicates the presence of the dark ring surrounding the spherical micelle in image (b).

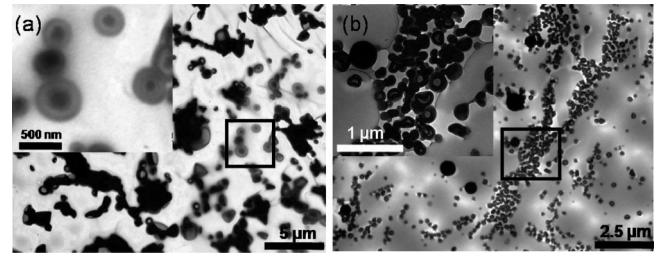

Figure 4. TEM micrographs of vesicles formed by B90V10 (a) and B87V13 (b) in dioxane/water mixtures (a = 5:3; b = 1:1). The particles were imaged on a Formvar-coated copper grid after cross-linking of the solutions (c = 0.25 wt %). The insets represent magnifications corresponding to the squares shown.

The plot of decay rates vs squared scattering vector does not show any strong angular dependence and the linear fit of the data passes through the origin, indicating the observation of real diffusive spherical particles.[50] Viscosity and

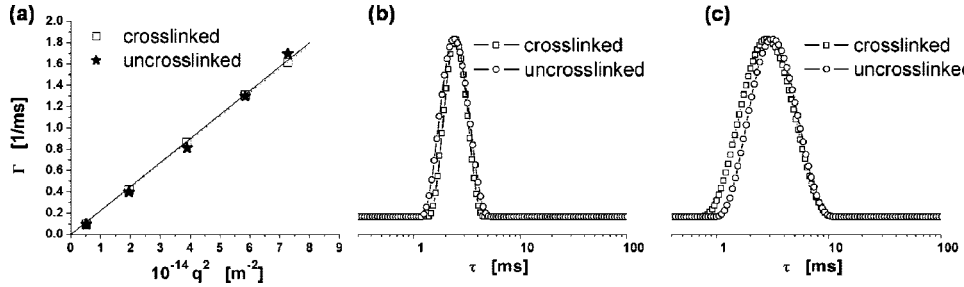

Figure 5. (a) Angular dependence of the decay rates of B80V20 before ($c = 0.25$ wt %) and after cross-linking ($c = 0.1$ wt %) in a dioxane/water mixture (1:1). (b) CONTIN plots (at 90°) before ($c = 0.25$ wt %) and after ($c = 0.1$ wt%) cross-linking of B87V13 in dioxane/water mixture (1:1). (c) CONTIN plots (at 90°) before ($c = 0.25$ wt %) and after ($c = 0.1$ wt %) cross-linking of B90V10 in dioxane/water mixture (5:3).

refractive index data from Nayak et al.[51] were used to correctly treat the DLS data in dioxane/water mixtures.

The DLS shows comparable slopes and diffusion coefficients (see Figure 2a) for B87V13 and B90V10 and correspondingly a similar distribution in the CONTIN plots (see Figure 2b). On the contrary, B80V20 has a significantly higher diffusion coefficient and a CONTIN plot shifted to lower decay times, indicating the presence of smaller aggregates.

The z-average hydrodynamic radius of B80V20 can be calculated from the slope of the linear fit to $\langle R_h \rangle_z = 64$ nm using the Stokes–Einstein equation. Cumulant analysis yields a polydispersity index of 1.05. The TEM analysis of the cross-linked sample shows spherical type micelles which exhibit a similar size range compared to the hydrodynamic radius obtained from DLS. A statistical analysis yields number-average and z-average radii of $\langle R \rangle_n = 48$ nm and $\langle R \rangle_z = 51$ nm, which are slightly lower than the z-average hydrodynamic radius. A lower value for the radius obtained from the TEM is expected and the difference to the z-average hydrodynamic radius appears reasonable when bearing the fact in mind, that the P2VP chains are collapsed in the dried state and not extended as in solution. Furthermore, the polybutadiene core is not swollen with solvent (dioxane) in the dried state and may thus be shrunken to some extent as well.

The micelles are well-defined and exhibit a moderately low polydispersity ($\langle R \rangle_w / \langle R \rangle_n = 1.04$). The magnified micelle in Figure 3b exhibits a dark ring surrounding the spherical micelle. This corona can be further elucidated by the section analysis, as presented in Figure 3c. The ring has an extension of ca. 3–5 nm and originates from the collapsed P2VP corona shielding the PB core of the micelle. The slightly different contrast of P2VP and PB is sufficient to be directly imaged, even without further staining (e.g., by I_2). Due to the low fraction of P2VP in the corona, the structures can be considered as crew-cut micelles.

The other two block copolymers with even shorter P2VP blocks show a different aggregation behavior at high water concentrations. The DLS data again exhibit no significant angular dependence, which is indicative of spherical particles (see Figure 2).

The determined particle radii are $\langle R_h \rangle_z = 159$ and 193 nm for B87V13 and B90V10, respectively. These aggregates are significantly larger than those formed by B80V20. B90V10 exhibits a broader distribution of decay times, reflecting the higher polydispersity with respect to B87V13. The polydispersities determined from the cumulant analysis (1.07 for B87V13 and 1.13 for B90V10) confirm this observation. The TEM micrographs (see Figure 4), obtained for both samples after cross-linking clearly show vesicles.

B90V10 exhibits larger vesicles and a broader size distribution. Additionally, some vesicles appear to contain a core, which may be an indication for multilamellar vesicular aggregates. The larger aggregates present on the images form during deposition, as they cannot be found in the DLS measurements. Aggregation of small particles into larger ones often occurs during the solvent evaporation process. This is why we always paid attention to the fact whether the structures found in TEM correspond to what can be found in DLS. It will be shown in the following section that the solution structures after cross-linking coincide with the ones before as concluded from the DLS data. B87V13, in contrast to B90V10, contains a small fraction of large compound micelles. Due to the appearance of vesicles in these two samples, one of them was selected for the later investigation of the phase transitions which occur at lower water concentrations (see below).

Cross-Linking. Before turning to the morphological transitions of the micellar system, the successful and facile cross-linking of different aggregate morphologies will be shown in the following. Generally, cross-linking of polybutadiene containing micellar aggregates can yield well-defined nanoobjects, which can find widespread use, i.e., as robust templates for inorganic materials. Herein, we present a new approach for the facile cross-linking of polybutadiene. Instead of γ-irradiation, which is a very noninvasive, however, not a readily available and expensive technique, an oil-soluble photo-cross-linker on phosphine oxide basis was used. The cross-linking can be conducted simply by mixing the micellar solution in dioxane/water mixtures with the photoinitiator and subsequent UV exposure. A coagulation of the structures and an intermicellar cross-linking was not observed, even not for higher concentrations of block copolymer up to 0.5 wt %. The hydrophobic UV initiator is presumably located in the polybutadiene phase after a short equilibration time.

Dynamic light scattering was used in order to analyze whether the cross-linking has any effect on the type of micellar aggregate formed. Figure 5 displays a comparison of the angular dependent decay rates and several CONTIN plots before and after cross-linking of different samples.

No major changes can be observed after cross-linking of the aggregates, independent of the aggregates shape, i.e. spherical micelle or vesicle. The decay rates for B80V20 essentially stay the same and the CONTIN plots for B87V13 and B90V10 neither exhibit significant changes. B90V10 shows a tiny shift toward smaller radii, indicating a slight contraction of the structures. Such small changes may however also be caused by the fitting procedure of the CONTIN algorithm in the evaluation of the autocorrelation functions.

After cross-linking, the particles were transferred into different solvents in order to prove the sufficient cross-linking and to explore their shape persistence upon changes in solvent quality. Figure 6 displays several TEM images obtained for the different diblock copolymers after cross-linking and transfer into ethanol or THF.

The images convincingly show that the cross-linked structures of the aggregates remain intact after transfer into different

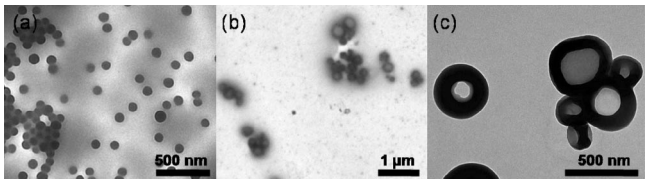

Figure 6. TEM micrographs of micelles and vesicles formed by B80V20 (a), B87V13 (b), and B90V10 (c). The aggregates were cross-linked and transferred into different solvents and then deposited on a Formvar-coated copper grid. Images (a) and (b) were acquired from THF solution, whereas image (c) was acquired from ethanol.

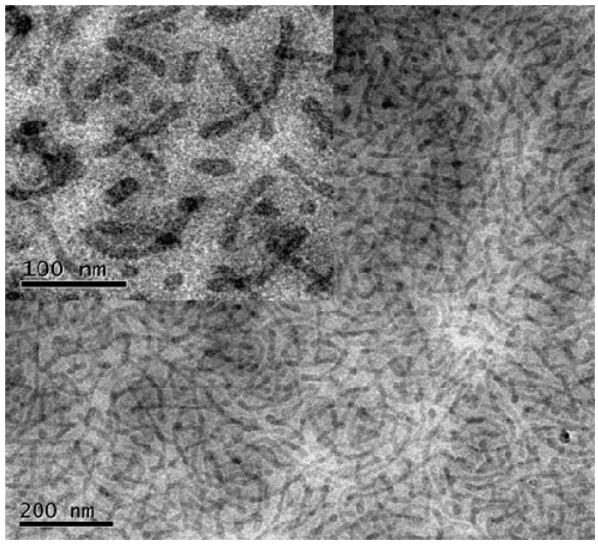

Figure 7. *Cryo*-TEM images obtained for a 1 wt % solution of B80V20 in THF. The inset shows a *cryo*-TEM image which was taken with a higher magnification at a different position.

solvents in which disassembly or a morphological transition is expected. After transfer, B80V20 still exhibits spherical micelles, whereas B87V13 and B90V10 show vesicles. The structures found coincide with the initial structures found in dioxane/water mixtures (Figures 3 and 4). The efficiency of the cross-linking can be ultimately confirmed by a comparison with the aggregates formed by un-cross-linked B80V20 in THF solution. DLS analysis of B80V20 in THF gave an indication for a fraction of larger aggregates. In order to analyze the structures, *cryogenic* TEM (*cryo*-TEM) measurements were performed. The concept of *cryo*-TEM in THF has recently been applied by our group to study the self-assembly behavior of complex polymeric particles in organic solvents.[47]

The *cryo*-TEM image in Figure 7 clearly exhibits cylindrical micelles of un-cross-linked B80V20 in THF. Similar results were obtained for B87V13 and B90V10. However, after cross-linking of certain micellar or vesicular aggregates in dioxane/water mixtures and subsequent transfer into THF, cylindrical micelles cannot be found anymore (see Figures 6, a and b). This ultimately confirms the successful cross-linking of the polymeric nanoparticles. The aggregation behavior of all PB-*b*-P2VP diblock copolymers in THF is unexpected in the first place as THF is a presumably good solvent for both blocks. Most probably, the slight selectivity of the "common" solvent THF toward the two block segments is sufficient to induce this aggregation.

In conclusion, the cross-linking of the particles can be easily performed for different kinds of aggregates. Additionally, the aggregates can be transferred into various solvents and the shape remains unaffected. Thus, the particles may, for instance, be applicable as catalyst carriers for inorganic nanoparticles in a wide range of solvents. In principle, the separation of cross-linked micelles or vesicles from a reaction mixture may be easily accomplished via ultrafiltration or centrifugation.

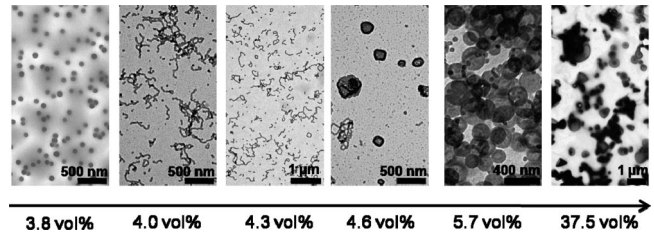

Figure 8. Phase evolution of crew-cut aggregates during the addition of water to a dioxane solution of B90V10 ($c = 0.5$ wt %). The TEM images were obtained after cross-linking.

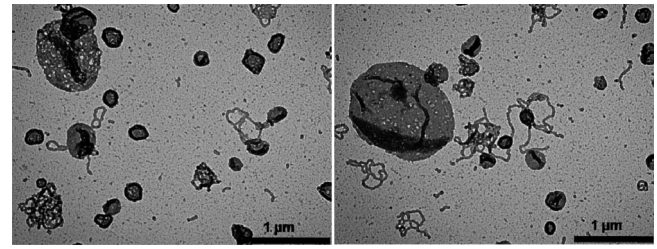

Figure 9. TEM micrographs obtained at the phase transition from branched cylindrical micelles to vesicles. The structures were cross-linked prior to imaging ($c = 0.5$ wt %, 4.6 vol % H_2O).

Phase Transitions. It is known from both experimental and theoretical work that block copolymers usually undergo phase transitions starting from spherical via cylindrical going to vesicular aggregates. In the case of PS-*b*-PAA block copolymers, the phase transitions can be induced by, e.g., adding water to an initial solution of the diblock copolymer in an organic solvent,[5,52–55] by changing the ionic strength,[56,57] addition of base[56] or acid[56,58] and to a small extent by temperature.[59]

B90V10 was selected for the investigation concerning the morphological transitions due to the observation of vesicles at high water concentrations and due to its composition, having the shortest P2VP block. Parallel DLS and TEM studies were conducted to identify the phase transitions. Figure 8 gives an overview of TEM micrographs obtained at different water contents.

All phase transitions occur at very low water contents of less than 10 vol %. The system shows well-developed spherical micelles for a very low water content of 3 vol %. A further increase induces a transition of the spherical micelles into branched wormlike micelles. The existence region of this type of aggregate is extremely narrow and wormlike micelles can only be found at water contents between 2 and 4 vol % in dioxane. The addition of more water to the system results in a transition of the branched wormlike micelles into vesicles. The transition occurs at a water content of 4.6 vol % under these particular conditions. At this point, a coexistence of long wormlike micelles with large globules and already developed vesicles can be found (see Figure 9). The coexistence of the different morphologies can be seen as an indication of a complex phase transition taking place at this point. The subsequently occurring vesicles still possess an internal structure inside their wall (see 4.6 and 5.7 vol % H_2O). This irregularly structured wall then disappears at higher water concentration and one ends up with standard vesicles at high water concentration. The polydispersity of the vesicles apparently increases with increasing water content, which might be caused by the decreasing solubility of the P2VP chains and its lower spatial requirement at higher water concentrations.

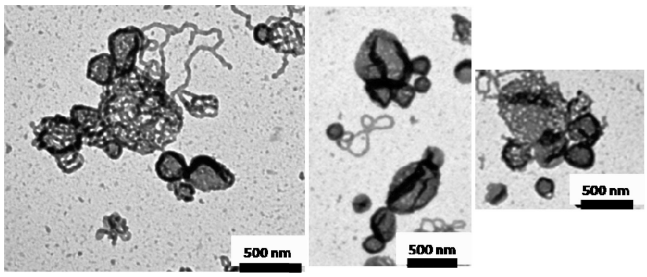

Figure 10. Magnification of TEM images obtained at the phase transition from wormlike micelles to vesicles.

Due to the appearance of large globules at the rod−vesicle transition and vesicles with internally structured walls, further attention was drawn to the phase transitions from branched cylindrical micelles to vesicles. The transition occurs in a completely different fashion than in the well-known crew-cut PS-*b*-PAA systems, investigated by Eisenberg and co-workers. In their case, the transition follows a two-step process. In the beginning, the cylinders transform into a lamellar structure, which then forms vesicles via a cuplike intermediate.[53] This mechanism finds some analogy with low molecular weight amphiphiles which show a similar transition mechanism, involving a metastable disklike bilayer structure.[60–62] Within this context, it should also be mentioned that Discher et al. recently observed the network formation of wormlike micelles of a symmetric non-crew-cut PB-*b*-PAA diblock copolymer via fluorescence microscopy. They identified a network-like structure as last morphology before the observation of vesicles and higher ordered vesicles.[63]

In this case, we propose the following pathway: in the beginning of the transition, the branched cylinders assemble into larger globules, whereas distinct lamellar structures cannot be found. These globules may be very large in size as can be seen in the right-hand image of Figure 9. Importantly, a formation of the large globules during the deposition can be excluded as they can be observed everywhere on the TEM grid, even in very sparsely covered areas. The hollow globules still show the wormlike cylindrical micelle features in their walls. In a following step, the vesicles are formed out of these hollow globules. However, the question arises how these globules or larger structures are able to form vesicles of significantly smaller size. A more detailed look at many images helps to solve this question. Figure 10 exhibits several magnifications of larger globules.

In the images presented, it can be seen that several smaller vesicles are connected to larger globules and network-like structures of wormlike micelles. Consequently, in order to complete the phase transition, these smaller vesicles must be released and completely separated from the larger globules and network-like aggregates. This observation can essentially explain how small vesicles are formed out of large globules. The large globules are unstable under the solvent conditions and do not lead to the formation of giant vesicles, but to the formation of small ones. The phase transition from wormlike micelles to vesicles can thus be reasonably understood. Upon further addition of water the rodlike features in the walls disappear and the cylinders in the walls of the small vesicles fuse to give unstructured vesicle walls in the end.

These results demonstrate that the phase transition in block copolymers may follow significantly different pathways. The appearance of a certain pathway may depend on the individual system. The mechanism shown here may be a result of the branched nature of the cylindrical micelles, which certainly facilitates the formation of large hollow globules as compared to linear cylindrical micelles.

Conclusion

The phase transitions and structures of crew-cut aggregates of polybutadiene-*block*-poly(2-vinylpyridine) were explored by combined DLS and TEM investigations. Depending on the block ratios and the added amount of water, differently shaped crew-cut aggregates are formed in dioxane/water mixtures. The morphologies change from spherical micelles via branched cylindrical micelles to vesicles with increasing water content. A new pathway for the transformation of cylindrical micelles into vesicles has been found. The cylinders assemble into large network-like structures and hollow globules and then release smaller vesicles upon completion of the phase transition.

The aggregates can be cross-linked via a simple photo-cross-linking method using a commercial UV photoinitiator, yielding stable nanoparticles of different architectures. It was shown that the stabilized nanoparticles can be transferred into different solvents under persistence of their shape, rendering them interesting for further applications in a large variety of solvents.

Acknowledgment. Denise Danz is acknowledged for the MALDI-ToF measurements and for her help in the synthesis of the block copolymers. This work was supported by the European Union within the Marie Curie RTN POLYAMPHI and by the DFG within the EUROCORES project BIOSONS. A.W. acknowledges financial support from the Bavarian Elite Support Program. R.S.Y. thanks the Bavarian Elite Network for a fellowship. A.E. acknowledges a grant from the Alexander von Humboldt Society.

References and Notes

(1) Li, C.; Buurma, N. J.; Haq, I.; Turner, C.; Armes, S. P.; Castelletto, V.; Hamley, I. W.; Lewis, A. L. *Langmuir* **2005**, *21*, 11026–11033.
(2) Antonietti, M.; Förster, S. *Adv. Mater.* **2003**, *15*, 1323–1333.
(3) Reiss, G. *Prog. Polym. Sci.* **2003**, *28*, 1107–1170.
(4) Förster, S.; Plantenberg, T. *Angew. Chem.* **2002**, *114*, 712–739.
(5) Shen, H.; Eisenberg, A. *Macromolecules* **2000**, *33*, 2561–2572.
(6) Yu, K.; Eisenberg, A. *Macromolecules* **1996**, *29*, 6359–6361.
(7) Choucair, A.; Lavigueur, C.; Eisenberg, A. *Langmuir* **2004**, *20*, 3894–3900.
(8) Terreau, O.; Luo, L.; Eisenberg, A. *Langmuir* **2003**, *19*, 5601–5607.
(9) Zhang, L.; Eisenberg, A. *J. Am. Chem. Soc.* **1996**, *118*, 3168–3181.
(10) Choucair, A. A.; Kycia, A. H.; Eisenberg, A. *Langmuir* **2003**, *19*, 1001–1008.
(11) Burke, S. E.; Eisenberg, A. *Langmuir* **2001**, *17*, 6705–6714.
(12) Yu, K.; Bartels, C.; Eisenberg, A. *Langmuir* **1999**, *15*, 7157–7167.
(13) Zhang, L.; Eisenberg, A. *Macromolecules* **1999**, *32*, 2239–2249.
(14) Kukula, H.; Schlaad, H.; Antonietti, M.; Förster, S. *J. Am. Chem. Soc.* **2002**, *124*, 1658–1663.
(15) Zhang, L.; Eisenberg, A. *Science* **1995**, *268*, 1728–1731.
(16) Borchert, U.; Lipprandt, U.; Bilang, M.; Kimpfler, A.; Rank, A.; Peschka-Suess, R.; Schubert, R.; Lindner, P.; Förster, S. *Langmuir* **2006**, *22*, 5843–5847.
(17) Choucair, A.; Soo, P. L.; Eisenberg, A. *Langmuir* **2005**, *21*, 9308–9313.
(18) Soo, P. L.; Luo, L.; Maysinger, D.; Eisenberg, A. *Langmuir* **2002**, *18*, 9996–10004.
(19) Luo, L.; Tam, J.; Maysinger, D.; Eisenberg, A. *Bioconjug. Chem.* **2002**, *13*, 1259–1265.
(20) Liu, S.; Armes, S. P. *Langmuir* **2003**, *19*, 4432–4438.
(21) Cai, Y.; Armes, S. P. *Macromolecules* **2004**, *37*, 7116–7122.
(22) Lee, A. S.; Butun, V.; Vamvakaki, M.; Armes, S. P.; Pople, J. A.; Gast, A. P. *Macromolecules* **2002**, *35*, 8540–8551.
(23) Lee, A. S.; Gast, A. P.; Butun, V.; Armes, S. P. *Macromolecules* **1999**, *32*, 4302–4310.
(24) Baines, F. L.; Armes, S. P.; Billingham, N. C.; Tuzar, Z. *Macromolecules* **1996**, *29*, 8151–8159.
(25) Regenbrecht, M.; Akari, S.; Förster, S.; Möhwald, H. *Surf. Interface Anal.* **1999**, *27*, 418–421.
(26) Krämer, E.; Förster, S.; Göltner, C.; Antonietti, M. *Langmuir* **1998**, *14*, 2027–2031.
(27) Selb, J.; Gallot, Y. *Makromol. Chem.* **1980**, *811*, 809–822.
(28) Selb, J.; Gallot, Y. *Makromol. Chem.* **1981**, *182*, 1513–1524.

(29) Gao, Z.; Varshney, S. K.; Wong, S.; Eisenberg, A. *Macromolecules* **1994**, *27*, 7923–7927.
(30) Yu, Y.; Eisenberg, A. *J. Am. Chem. Soc.* **1997**, *119*, 8383–8384.
(31) Shen, H.; Zhang, L.; Eisenberg, A. *J. Am. Chem. Soc.* **1999**, *121*, 2728–2740.
(32) Yao, X.; Chen, D. Y.; Jiang, M. *J. Phys. Chem. B* **2004**, *108*, 5225–5229.
(33) Antonietti, M.; Heinz, S.; Schmidt, M.; Rosenauer, C. *Macromolecules* **1994**, *27*, 3276–3281.
(34) Park, S.-Y.; Chang, Y.-J.; Farmer, B. L. *Langmuir* **2006**, *22*, 11369–11375.
(35) Calderara, F.; Riess, G. *Macromol. Chem. Phys.* **1996**, *197*, 2115–2132.
(36) Peng, H. S.; Chen, D. Y.; Jiang, M. *Langmuir* **2003**, *19*, 10989–10992.
(37) Klingelhöfer, S.; Heitz, W.; Greiner, A.; Oestreich, S.; Förster, S.; Antonietti, M. *J. Am. Chem. Soc.* **1997**, *119*, 10116–10120.
(38) Förster, S.; Antonietti, M. *Adv. Mater.* **1998**, *10*, 195–217.
(39) Tsutsumi, K.; Funaki, Y.; Hirokawa, Y.; Hashimoto, T. *Langmuir* **1999**, *15*, 5200–5203.
(40) Platonova, O. A.; Bronstein, L. M.; Solodovnikov, I. M.; Yanovskaya, I. M.; Obolonkova, P. M.; Valetsky, P. M.; Wenz, E.; Antonietti, M. *Colloid Polym. Sci.* **1997**, *275*, 426–431.
(41) Lu, J.; Yi, S. S.; Kopley, T.; Qian, C.; Liu, J.; Gulari, E. *J. Phys. Chem. B* **2006**, *110*, 6655–6660.
(42) Prochazka, K.; Baloch, M. K.; Tuzar, Z. *Makromol. Chem.* **1979**, *180*, 2521–2523.
(43) Guo, A.; Liu, G. J.; Tao, J. *Macromolecules* **1996**, *29*, 2487–2493.
(44) O'Reilly, R. K.; Hawker, C. J.; Wooley, K. L. *Chem. Soc. Rev.* **2006**, *35*, 1068–1083.
(45) Liu, Y.; Abetz, V.; Müller, A. H. E. *Macromolecules* **2003**, *36*, 7894–7898.
(46) Erhardt, R.; Böker, A.; Zettl, H.; Kaya, H.; Pyckhout-Hintzen, W.; Krausch, G.; Abetz, V.; Müller, A. H. E. *Macromolecules* **2001**, *34*, 1069–1075.
(47) Walther, A.; André, X.; Drechsler, M.; Abetz, V.; Müller, A. H. E. *J. Am. Chem. Soc.* **2007**, *129*, 6187–6198.
(48) Maskos, M. *Polymer* **2006**, *47*, 1172–1178.
(49) Provencher, S. W. *Makromol. Chem.* **1979**, *180*, 201–209.
(50) Stepanek, P. *J. Chem. Phys.* **1993**, *99*, 6384–6393.
(51) Nayak, J. N.; Aralaguppi, M. I.; Naidu, B. V. K.; Aminabhavi, T. M. *J. Chem. Eng. Data* **2004**, *49*, 468–474.
(52) Shen, H.; Eisenberg, A. *J. Phys. Chem. B* **1999**, *103*, 9473–9487.
(53) Chen, L.; Shen, H.; Eisenberg, A. *J. Phys. Chem. B* **1999**, *103*, 9488–9497.
(54) Yu, Y.; Zhang, L.; Eisenberg, A. *Langmuir* **1997**, *13*, 2578–2581.
(55) Terreau, O.; Bartels, C.; Eisenberg, A. *Langmuir* **2004**, *20*, 637–645.
(56) Zhang, L.; Eisenberg, A. *Macromolecules* **1996**, *29*, 8805–8815.
(57) Zhang, L.; Shen, H.; Eisenberg, A. *Macromolecules* **1997**, *30*, 1001–1011.
(58) Zhang, L.; Eisenberg, A. *J. Pol. Sci. B* **1999**, *37*, 1469–1484.
(59) Desbaumes, L.; Eisenberg, A. *Langmuir* **1999**, *15*, 36–38.
(60) Farquhar, K. D.; Misran, M.; Robinson, B. H.; Steyltler, D. C.; Morini, P.; Garret, P. R.; Holzwarth, J. F. *J. Phys.: Condens. Matter* **1996**, *8*, 9397–9404.
(61) Edward, K.; Almgren, M.; Bellare, J.; Brown, W. *Langmuir* **1989**, *5*, 473–478.
(62) O'Connor, A. J.; Hatton, A. T.; Bose, A. *Langmuir* **1997**, *13*, 6931–6940.
(63) Geng, Y.; Ahmed, F.; Bhasin, N.; Discher, D. E. *J. Phys. Chem. B* **2005**, *109*, 3772–3779.

MA7026148